JOURNAL OF EXTRACELLULAR VESICLES
2019, VOL. 9, 1703249
https://doi.org/10.1080/20013078.2019.1703249

Taylor & Francis
Taylor & Francis Group

Neuronal-derived extracellular vesicles are enriched in the brain and serum of HIV-1 transgenic rats

Raghubendra Singh Dagur[a], Ke Liao [a], Susmita Sil[a], Fang Niu [a], Zhiqiang Sun[b], Yuri L. Lyubchenko[b], Eric S. Peeples [c], Guoku Hu[a] and Shilpa Buch [a]

[a]Department of Pharmacology and Experimental Neuroscience, University of Nebraska Medical Center, Omaha, NE, USA; [b]Department of Pharmaceutical Sciences, University of Nebraska Medical Center, Omaha, NE, USA; [c]Department of Pediatrics, University of Nebraska Medical Center, Omaha, NE, USA

ABSTRACT

Despite the efficacy of combination antiretroviral therapy (ART) in controlling human immunodeficiency virus (HIV-1) replication, cytotoxic viral proteins such as HIV-1 transactivator of transcription (Tat) persist in tissues such as the brain. Although HIV-1 does not infect neuronal cells, it is susceptible to viral Tat protein-mediated toxicity, leading to neuroinflammation that underlies HIV-associated neurocognitive disorders (HAND). Given the role of extracellular vesicles (EVs) in both cellular homoeostasis and under pathological conditions, we sought to investigate the alterations in the quantity of neuronal-derived EVs in the brain – as defined by the presence of cell adhesion molecule L1 (L1CAM) and to evaluate the presence of $L1CAM^+$ EVs in the peripheral circulation of HIV-1 transgenic (HIV-1 Tg) rats. The primary goal of this study was to investigate the effect of long-term exposure of HIV-1 viral proteins on the release of neuronal EVs in the brain and their transfer in the systemic compartment. Brain and serum EVs were isolated from both wild type and HIV-1 Tg rats using differential ultracentrifugation with further purification using the Optiprep gradient method. The subpopulation of neuronal EVs was further enriched using immunoprecipitation. The current findings demonstrated increased presence of $L1CAM^+$ neuronal-derived EVs both in the brain and serum of HIV-1 Tg rats.

ARTICLE HISTORY
Received 25 July 2019
Revised 6 November 2019
Accepted 5 December 2019

KEYWORDS
Extracellular vesicles; HIV-1; neuronal EVs; serum EVs; brain EVs

Introduction

While antiretroviral therapy (ART), the cornerstone for treatment of HIV-1 infection, has been effective in controlling peripheral viraemia in HIV-1 infected individuals, inability of some of these drugs to cross the blood-brain barrier (BBB), however, leads to persistence of low-level virus replication in the central nervous system (CNS) [1,2]. Additionally, ART treatment fails to impact the production of early cytotoxic viral proteins such as Tat, thereby leading to a neuroinflammatory milieu in the brain, which is one of the hallmark features of HIV-associated neurological disorders (HAND) [3,4]. HAND affects almost 30–60% of infected individuals and comprises clinical symptomatology ranging from asymptomatic to minor cognitive motor disorders [5–8]. Based on the understanding that the cognitive decline associated with HAND reflects neuronal damage and the fact that neurons are not infected by HIV-1, mechanism(s) other than direct infection are likely suggestive of the underlying neuropathogenesis.

Recent evidence has implicated the role of extracellular vesicles (EVs) as contributors to the pathogenesis of various neurodegenerative diseases including Alzheimer's (AD) and Parkinson's diseases (PD) [9–12]. EVs, including exosomes (50–200 nm) are composed of membrane proteins and lipids, as well as cytoplasmic components of the cell from which they originate, such as mRNA and miRNA, organelles or infectious particles [13–18]. Many studies have suggested a bidirectional transport of EVs from the brain to the systemic circulation via the BBB [19–21]. For example, systemic delivery of EVs from dendritic cells (DCs) loaded with the small interfering RNA (siRNA) were used as therapeutic vehicles to treat a mouse model of Alzheimer's disease [21], suggesting thereby the ability of these vehicles to cross the BBB and deliver the siRNA cargo into target cells for specific gene knockdown [22]. In another study EVs derived from a mouse lymphoma cell line were demonstrated to deliver curcumin across the BBB into microglial cells via the intranasal administration route to attenuate neuroinflammation and autoimmune responses in an experimental autoimmune encephalomyelitis (EAE) model [23].

CONTACT Shilpa Buch sbuch@unmc.edu; Guoku Hu guoku.hu@unmc.edu Department of Pharmacology and Experimental Neuroscience, University of Nebraska Medical Center, Omaha, NE 68198-5880, USA

Over the past years search for brain-derived EVs as peripheral non-invasive biomarker(s) for neurodegenerative diseases has gained momentum [24,25]. Based on the premise that in the CNS the expression of cell adhesion molecule L1CAM is primarily restricted to neurons, the presence of this protein in the exosomes demonstrates its neuronal origin [26–28]. EVs derived from cultured cortical neurons have been demonstrated to exhibit cell adhesion molecule L1 (L1CAM) on their surface, with implications for various neurodegenerative diseases [28]. In fact, increased release and transit of L1CAM+ EVs via the blood brain barrier has been reported in the plasma of HIV+ patients, suggesting their role as a liquid biopsy biomarker [29]. Additionally, L1CAM+ EVs have also been identified in both melanoma cells [30], and in ovarian cancer [31]. Neuronal enrichment of EVs has the benefit of improving the signal to noise ratio, increase the measurement sensitivity, lower the detection threshold (by providing an enriched fraction containing higher concentrations of target molecule compared with plasma or total EVs), and better reflect the pathophysiological processes occurring in the CNS. Elegant studies have demonstrated the presence of p-T181-tau and p-T231-tau in both plasma and serum-derived L1CAM$^+$ EVs, that were not detectable in either the serum or plasma samples even using a sensitive electrochemiluminescence-based assay [25,28,29]. Intriguingly, Lamontagne-Proulx et al. have also identified specific signature proteins in the plasma EVs that could reliably differentiate control subjects from mild or moderate in patients with PD [32]. These studies thus suggest that EVs and their cargo not only play a role in the onset of various diseases but could also serve as excellent indicators for disease progression.

In the present study, we employed the HIV-1 transgenic (Tg) rat model that constitutively expresses 7 of the 9 HIV-1 proteins including Tat, to evaluate the effect of viral proteins on the release of neuronal-origin L1CAM$^+$ EVs in both the extracellular space of the brain as well as serum. Our findings suggest increased release of neural-derived EVs in both brain as well as in the serum of HIV-1 Tg rats compared to the wild type (WT) controls.

Materials and methods

Animals

HIV-1 Transgenic rats were purchased from Harlan Laboratories (Indianapolis, Indiana, USA) and were generated using a non-infectious provirus expressing HIV-1 viral proteins, such as Tat, Env, Rev, Nef and Vif. In these animals, viral proteins are continually expressed throughout the lifespan of the animal. Presence of Nef and the other viral proteins has been suggested in the blood, lymph nodes, spleen and CNS of these HIV-1Tg rat [33–35]. In these Tg animals, expression of mRNA levels of viral proteins in the spinal cord, cerebellum, and striatum were found to be significantly higher in the older rats compared with younger animals, thus suggesting age-dependent differential expression of various HIV viral proteins [34]. Given the higher prevalence of HIV-associated neurocognitive impairment in women versus men (52% vs 41%) [36], female animals were evaluated in the present study. Female HIV-1 transgenic Sprague Dawley rats (HIV-1 Tg, F344; 12–18 months age) were selected due to the fact that the HIV-1 Tg rats express increased levels of viral proteins by 11–12 months of age in the brain that is accompanied with the gradual development of AIDS-related neuropathologies [34]. Age and background-matched wild-type controls (Fischer 344 WT) were also used in the study. Animals were housed in clean polypropylene cages under conditions of constant temperature and humidity, with a 12 h light and 12 h night cycle, during which time they had free access to food and water ad libitum. All animal procedures were performed following the protocols approved by the University of Nebraska Medical Centre (UNMC) Institutional Animal Care and Use Committee.

Isolation of EVs from hemibrain

Whole brains were extracted from Fischer 344 WT and HIV-1 Tg female rats (n = 5 each group) at 12–18 months of age following rapid decapitation and kept frozen at −80° C until further processing. Hemibrains were homogenized in 10–15 mL of activating solution consist of Hibernate A medium with proteolytic enzyme papain (20 units/mL) and incubated at 37°C for ~30 min on gentleMACS Octo Dissociator with heaters (Miltenyi Biotec, USA) using inbuilt 37C_ABDK_1 Program. Following homogenization, the suspension was centrifuged at 300 x g for 10 min, and then at 2000 x g for 10 min at 4°C to eliminate tissue fragments and cells, dead cells and debris, respectively. Supernatants were then filtered through 0.8 μm filters, and further centrifuged at 10,000 x g for 30 min to discard unwanted large vesicles. The supernatant was then filtered through 0.2 μm filters and ultracentrifuged at 100,000 x g for 70 min at 4°C in an SW32 Ti rotor to concentrate small EVs. EV pellets were resuspended in 500 μL of 0.25 M sucrose buffer [10 mM Tris, pH 7.4] for gradient purification. Top-loaded sedimentation gradients were performed on 5, 10, 20 and 40% iodixanol (Optiprep; Cosmo Bio USA) gradient as previously described [37,38]. Briefly, three mL of high-density iodixanol (40%) was first transferred to the bottom of a 14 mL ultracentrifugation tube. Subsequently, 20, 10 and 5% of

iodixanol (each 3 mL) were layered, and 500 µL of resuspended EVs were loaded on top. Gradients were ultracentrifuged at 100,000 x g in an SW40 Ti rotor for 18 h. After discarding 500 µL from the top, 12 fractions of 1 mL were taken from the top of the gradient (named F1-F12), diluted in phosphate-buffered saline (PBS), and pelleted again for one hour at 100,000 x g in an SW40 Ti rotor to get rid of iodixanol from the samples. Alternatively, iodixanol fractions were pooled and resuspended in sterile 1 x PBS, followed by ultracentrifugation for 70 min at 100,000 x g in an SW32 Ti rotor (Beckman) to pellet EVs for the removal of iodixanol for immunoprecipitation of L1CAM$^+$ neuronal EVs [29].

Isolation of EVs from serum

Serum collection and EV isolation from blood were in accordance with guidelines published previously [39,40]. Briefly, blood was collected in 6 mL serum tubes (BD Vacutainer, USA) from 344 WT and HIV-1 Tg rats at 12–18 months of age by cardiac puncture after euthanizing animals. We had 8–10 female rats in each group. Blood was centrifuged at room temperature at 2500 x g for 15 min to collect serum and subsequently underwent another centrifugation step at 2500 x g for 15 min in a clean plastic tube. EVs were isolated by ultracentrifugation and purification by iodixanol density gradient, as reported previously [41,42].

Enrichment of L1CAM$^+$ EVs from brain-and serum-EVs

Enrichment of L1CAM$^+$ EVs was performed by immunoprecipitation using a biotinylated antibody specific for neuronal surface marker to isolate a subpopulation of L1CAM$^+$ EVs as described previously [28,43,44]. Briefly, 50% of pooled F1-F7 fractions from the brain fraction and F6-F10 fractions from the serum fraction were incubated overnight at 4°C with 4 µg of rabbit anti-rat L1CAM biotinylated antibody (LS Bio, USA; LS-C470565) in 100 µL of 3% bovine serum albumin (BSA) and bound to 25 µL of Streptavidin-plus ultra-link resin (ThermoFisher, USA) for 1 h at 4°C. After centrifugation at 3000 x g for 5 min at 4°C and removal of the supernatant (L1CAM$^-$ EV fraction), pellet were suspended in 90 µL of 0.1 M glycine-HCl (pH 2.8) to release EVs in the supernatant and neutralized with 10 µL of 1 M Tris-HCl (pH 8.0). Neuron-derived EVs were counted using zeta view and were subsequently used for western blotting.

Atomic force microscopy

Atomic force microscopy was performed to characterize the topography of extracellular vesicles as described previously [14]. Briefly, 20µL (9–12 × 10^{11} EVs/mL) of EV sample was deposited on APS mica for 20 min at room temperature. Then 200 µL of the PBS buffer was added to the sample. The sample was then subjected to atomic force microscopy (AFM) imaging using the Asylum Research MFP3D (Santa Barbara, CA, USA) instrument. Imaging was performed in tapping mode at room temperature. An MSNL probe with cantilever "E" (Bruker Corporation) was employed for imaging. The nominal spring constant of the MSNL "E" cantilevers was ~0.1 N/m.

Zetaview tracking analysis

Nanoparticle tracking analysis (NTA) was performed using ZetaView Nanoparticle Tracking Analyser (Particle Metrix, Germany) and its corresponding software (ZetaView 8.04.02 SP1) to analyse EVs isolated from brain and serum samples, as published previously [45]. Briefly, 100 nm polystyrene nanostandard particles were used to calibrate the instrument before sample readings. Cell quality check and instrument alignment and focus were first performed prior to ZetaView for sample measurements using the software. For video acquisition, camera setting sensitivity was set to 85, shutter speed of 100 and a frame rate of 30 were used according to the system's software guidance. For each sample, 1 mL of the sample, diluted in 0.20 µm filtered PBS was loaded into the cell. The instrument measured each sample at 11 different positions throughout the cell, with 2 cycles of readings at each position. After automated analysis and removal of any outliers from the 11 positions, the size (diameter in nm) and the concentration (particles/mL) of the sample was calculated by the machine software. Measurement data from the Zeta View were analysed using the corresponding Zeta view software, and Microsoft Excel 2016. Final concentration was calculated by multiplying the observed concentration with the dilution factor.

Immunoblot analysis

EVs derived from equal amount (brain) and equal volume (serum) were lysed in 10x RIPA lysis buffer [150 mM NaCl, 1% Triton X-100, 50 mM Tris (pH 7.6), 0.1% SDS, 5 mM EDTA, 0.5% sodium deoxycholate] with the addition of HALT protease and phosphatase inhibitor. Proteins were extracted by sonication. For confirmation of EV proteins in purified lysates, 5X Laemmli sample buffer [10% SDS, 250 mM Tris pH 6.8, 1 mg/mL bromophenol

blue, 0.5 M DTT, 50% glycerol, 5% BME] was added to EVs. For immunoblot, proteins were electrophoresed in a sodium dodecyl sulphate-polyacrylamide gel (10–12%) under reducing conditions followed by transfer to PVDF membranes. Blots were probed with Alix (Abcam, USA); TSG101 (Abcam, USA); CD9 (Abcam, USA); Calnexin (Sigma, USA); L1CAM (LifeSpan Biosciences, USA), and βIII Tubulin (Biolegend, USA). The secondary antibodies were HRP conjugated to goat anti-mouse (Santa Cruz, USA)/rabbit IgG (Santa Cruz, USA). Images were acquired on FluorChem M FM0243 (Protein Simple, USA).

Statistical analysis

Significant differences in total EVs, neuronal-origin EVs harvested from WT and HIV-1 Tg brains and sera were determined by unpaired parametric student's t-test with Welch's correction and as mentioned in the respective figure legends.

Results

Purification and characterization of EVs from brain extracellular space

EVs were isolated from brain extracellular space by enzymatic digestion, differential centrifugation, and purification by Optiprep density gradient centrifugation as shown in the schematic in Figure 1(a). Size distribution assessed by zeta view revealed that 90% of particles distributed in the range of 50 to 200 nm, with a peak at ~110 nm. The observed heterogenicity in the size of particles is shown in a representative captured image from the video acquired on zeta view (Figure 1(b)). More than 95% of EVs with a size range of 50–200 nm were present in fractions F1-F7 (Figure 1(c)). The topography of F1-F7 EVs was assessed under the tapping mode by immobilizing vesicles on positively charged APS-mica surface for atomic force microscopy (AFM) analysis. Intact EVs that could be immobilized electrostatically presented a median size of 26.9 nm in height (Figure 1(d)). Western blotting of brain-derived EVs demonstrated positivity for exosome-enriched proteins Alix, TSG 101 and CD9 specifically in F1-F7 fractions and negative for endoplasmic reticulum protein calnexin. Brain-lysate was used as a positive control for calnexin (Figure 1(e)).

Neuronal-derived EVs are enriched in the brains of HIV-1 transgenic rats

Based on the premise that L1CAM$^+$ neuron-derived EVs are enriched in neurodegenerative diseases, we next sought to investigate alterations in L1CAM$^+$ EVs of neuronal origin ex vivo in the context of HIV-1 viral proteins. To check the neuronal origin of EVs, the subpopulation of L1CAM$^+$ EVs were immunoprecipitated from pooled F1-F7 fractions of EVs isolated from the brain lysates of HIV-1 Tg and WT using biotinylated antibodies against the neuronal surface marker. Neural cell adhesion molecule L1CAM was selected owing to its high and relatively specific expression in neural tissues [28,29]. The results from zeta-view demonstrated increased numbers of EVs in the pooled fractions (F1-F7) of HIV-1 Tg rats compared with that from the WT rats; this however, was not statistically significant (Figure 2(a)). Similarly, there were significantly increased numbers of L1CAM$^+$ EVs isolated from pooled F1-F7 fractions from HIV-1 Tg rats (mean value of 3.71 x 10^6/mg [range 4.86 × 10^5 to 1.01 × 10^7 EVs/mg]) compared with those isolated from pooled fractions of WT rats (mean value of EVs 3.71 x 10^5/mg [range 3.01 × 10^5 to 4.36 × 10^5) (Figure 2(b)). Pooled F1-F7 EVs and L1CAM$^+$EVs from HIV-1 Tg rats had a similar size distribution as the WT rats (range ~ 50 to 200 nm; Figure 2(c)). The concentration of L1CAM$^+$EVs however, was noticeably higher in HIV-1 Tg rats (mean value 1.84 × 10^4 EVs/mg) compared with the WT rats (1.85 x 10^5 EVs/mg; Figure 2(d)). We also confirmed the presence of L1CAM on EVs using antibodies against L1CAM tagged with biotin by western blotting (Figure 2(e)). Similar to previous studies, we observed cleaved form (~70, ~55 and ~30 kDa) of L1CAM in L1CAM$^+$ EVs [46,47]. Further, we confirmed the presence of another neuronal marker βIII Tubulin as well as exosomal markers TSG101 and CD9 on the L1CAM$^+$ EVs (Figure 2(e)). For Western blotting L1CAM$^+$ EVs derived from equal amount of brains were lysed in RIPA lysis buffer and loaded onto the gels. For normalization of EVs, brain lysates from both WT and HIV-1 Tg rats were probed with β-actin (Figure 2(f)). Densitometry of neuronal proteins and exosome proteins in L1CAM$^+$ EVs fraction revealed increased expression of L1CAM in HIV-1 Tg rats compared with the WT controls when normalized with the respective brain-lysate (input) (Figure 2(g)).

Purification and characterization of extracellular vesicles from rat serum

We next sought to investigate whether, similar to an increase in neuronal EVs in the brain of HIV-1 Tg rats, there was also an increase in L1CAM$^+$ EVs in the serum. We first isolated and purified EVs from the serum using a protocol similar to that for the brain-

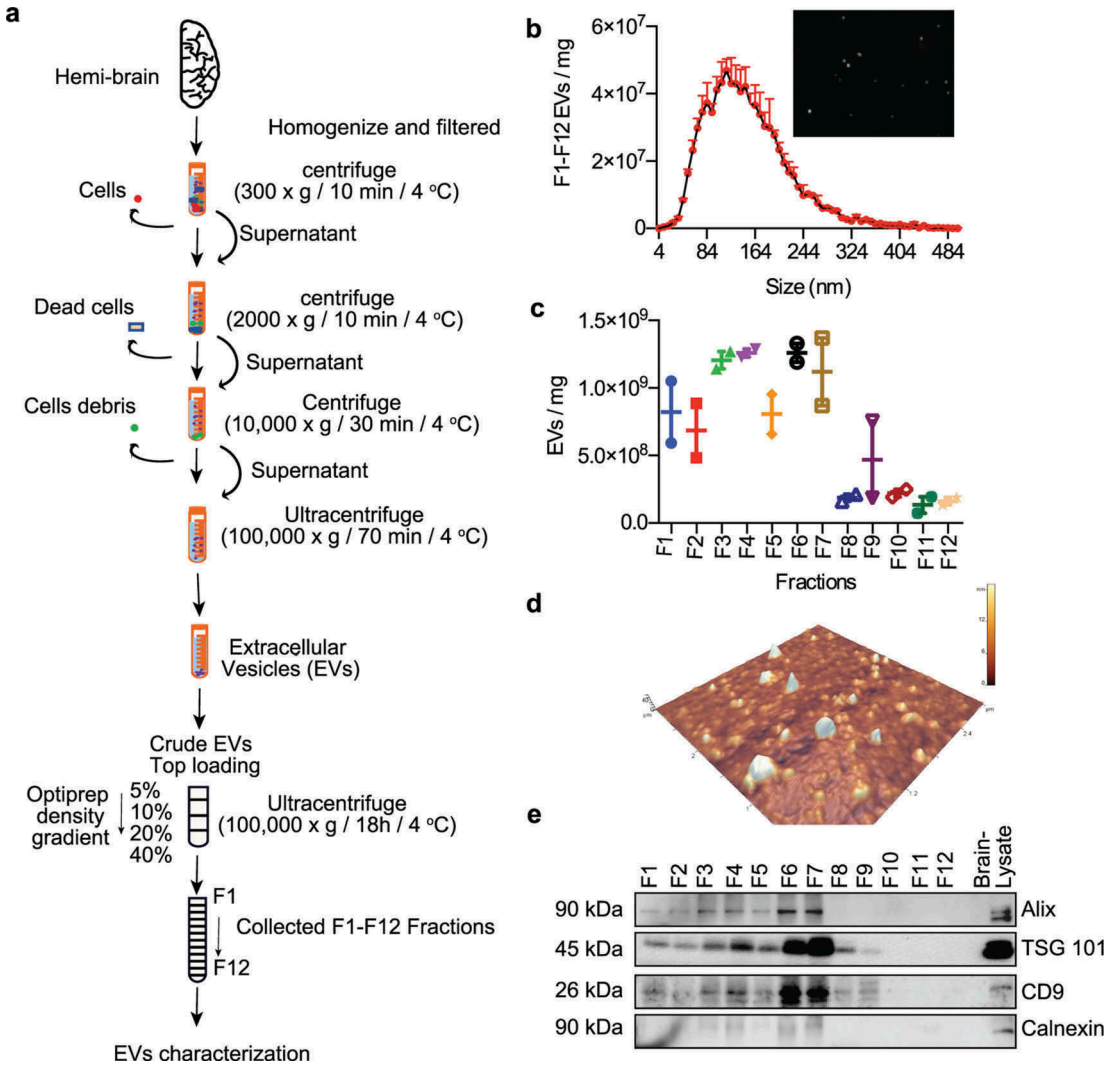

Figure 1. Characterization of brain-derived EVs: (a) Extracellular vesicles (EVs) were isolated from the brain of WT rats (n = 2) by enzymatic digestion and followed by series of centrifugation. For the purification, EVs were top-loaded on a 5–40% iodixanol and ultracentrifuge at 100,000 g for 18 h. Twelve 1 mL fractions (F1–F12) were collected. (b) Size distribution of EVs for the size range 4–500 nm of F1-F12 fraction from 2 WT- rats are shown. Inset image showing EVs morphology captured from the video in zeta view. (c) The graph shows the actual concentration of each fraction (F1-F12) assessed by zeta view after adjusting for dilutions. (d) Topographic profiling of F1-F7 EVs using atomic force microscopy (AFM) under tapping mode revealed a heterogeneous population of spherical particles. (e) Western blot images show protein expression from each fraction (F1-F12) for the presence of EV-associated proteins ALIX, TSG101 and CD9 exosome marker and non-exosome marker calnexin.

derived EVs as summarized in Figure 3(a). The findings from zeta view demonstrated a more than 90% distribution of particle size in the range of 50 to 200 nm with a peak at ~84 nm. Representative morphology of the EVs is shown in the inset (Figure 3(b)). More than 95% of EVs (ranging 50–200 nm) were present in fractions F6-F10 (Figure 3(c)). Morphology of EVs (F6-F10) was further assessed using AFM and showed heterogeneous topography of EVs (Figure 3(d)). Additionally, western blot was run to confirm the presence of exosomes in EVs and results showed that serum-derived EVs were positive for exosome-enriched proteins Alix, TSG 101 and CD9 specifically in fractions F6-F10 (Figure 3(e)).

Sera of HIV-1 Tg rats are enriched for neuronal origin EVs

Based on the premise that L1CAM$^+$ neuron-derived EVs are released in the serum in neurodegenerative diseases, we sought to investigate alterations in the quantity of circulating L1CAM$^+$ EVs *in vivo* in HIV-1 Tg compared to WT rats. Given the relative specificity of L1CAM to neural tissue, we started with pooled sera of 3–4 WT rats to ensure and maximize the yield of EVs to identify L1CAM$^+$ EVs and to assess whether EVs of neuronal origin were present in the serum.

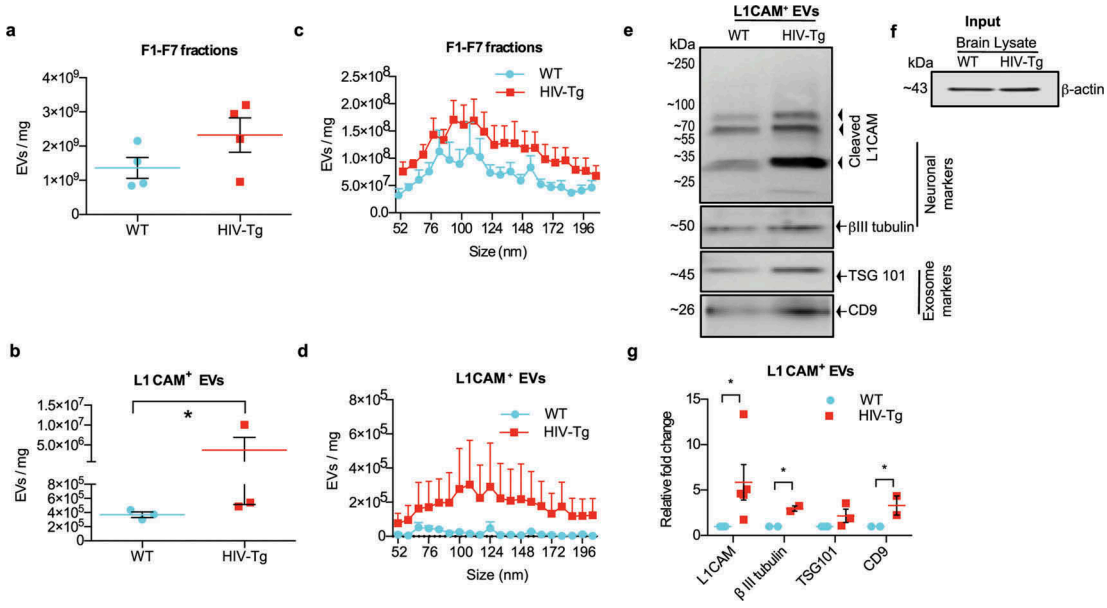

Figure 2. Neuronal-derived EVs are enriched in the brain of HIV-1 transgenic rats. (a) Graph showing the concentration of pooled F1-F7 fractions obtained from the brains of WT and HIV-Tg rats ($n = 4$), as evaluated by zeta-view. Equal amounts of brains from WT and HIV-1 Tg rats were used as the starting material to isolate total EVs. All conditions and dilutions were kept identical in both the groups (Wt and HIV-1 Tg) for further isolation of F1-F7 EVs and for L1CAM$^+$ EVs. * $p < 0.05$ by unpaired parametric student's t-test with Welch's correction. (b) Graph shows the actual concentration of EVs in the L1CAM$^+$ EVs fractions obtained by immunoprecipitation of pooled F1-F7 fractions of WT and HIV-1 Tg rats ($n = 3$), evaluated by zeta view. (c) Size distribution of F1-F7 fractions, and (d) L1CAM$^+$EVs was examined by nano track analysis using zeta view. Figures depict the actual concentration of EVs by adjusting for the dilution factor in the range of 50–200 nm. (e) Western blot images showing increased expression of neuronal markers (L1CAM, βIII tubulin) in L1CAM$^+$ EVs from HIV-1 Tg rat compared to L1CAM$^+$ EVs from WT rat ($n = 5$ each group). L1CAM$^+$ EVs derived from the brains (equal weights) from each group were loaded onto the gel. Representative L1CAM$^+$ EVs from one WT and one HIV-1 Tg rat are shown. CD9, TSG101 were used as a positive control for exosomes. (f) Brain lysate was used as input (1% of total brain lysate) and β-actin from brain lysates (input) was used as endogenous control for the brain-derived EVs. (g) Densitometry of proteins in L1CAM$^+$EVs fractions of WT and HIV-1 Tg rats normalized with brain lysate β actin (input). Graph for L1CAM expression shows densitometry of ~55 kDa band. *$p < 0.05$ by multiple t-test using the Holm-Sidak method.

For this, we pooled equal amount of sera from WT and HIV-1 Tg rats and counted the numbers of F6-F10 EVs and L1CAM$^+$EVs isolated from total EVs as well as pooled F6-F10 fractions, respectively. We observed increased EV concentration in the F6-F10 fractions isolated from the sera of HIV-1 Tg rats, with mean value of 1.35×10^{10} EVs/mL (range 9.8×10^9 to 1.92×10^{10} EVs/mL) in HIV-1 Tg compared with WT mean value 6.27×10^9 EVs/mL (range from 2.0×10^9 to 1.01×10^{10} EVs/mL) (Figure 4(a)). We also observed an increase in the L1CAM$^+$ neuronal EVs in HIV-1 Tg rats with mean value 2.51×10^8 EVs/mL (range 3.26×10^7 to 5.81×10^8 EVs/mL) as compared to the WT mean value 1.29×10^8 EVs/mL (range 2.08×10^7 to 2.96×10^8 EVs/mL). The difference between the two groups, however, was not statistically significant (Figure 4(b)). The F6-F10 pooled EVs (Figure 4(c)) and L1CAM$^+$ EVs (Figure 4(d)) from HIV-1 Tg rats had a size distribution similar to that of the WT rats, in the range of 50 nm to 200 nm, with median diameters of ~100 nm for F6-F10 EVs and ~110 nm for L1CAM$^+$ EVs. The concentration of each size, however, was considerably higher in the HIV-1 Tg group (Figure 4c,d). The results from western blots showed increased expression of L1CAM in HIV-1 Tg L1CAM$^+$ EVs compared to WT animals with a concomitant increase in the expression of another neuronal marker βIII Tubulin (Figure 4e,f). Similar to brain L1CAM$^+$ EVs, serum L1CAM$^+$EVs also displayed L1CAM fragments of ~70, ~55 and ~30 kDa. Exosome markers were also confirmed in L1CAM$^+$ EVs using exosome markers TSG 101 and CD9 (Figure 4e,f).

Discussion

The advent of highly active antiretroviral drugs has significantly reduced the incidence of most severe forms of neurocognitive impairment, including HIV-1-associated dementia; however, milder forms of neurocognitive impairment continue to afflict ~ 40 and 60% of HIV-1

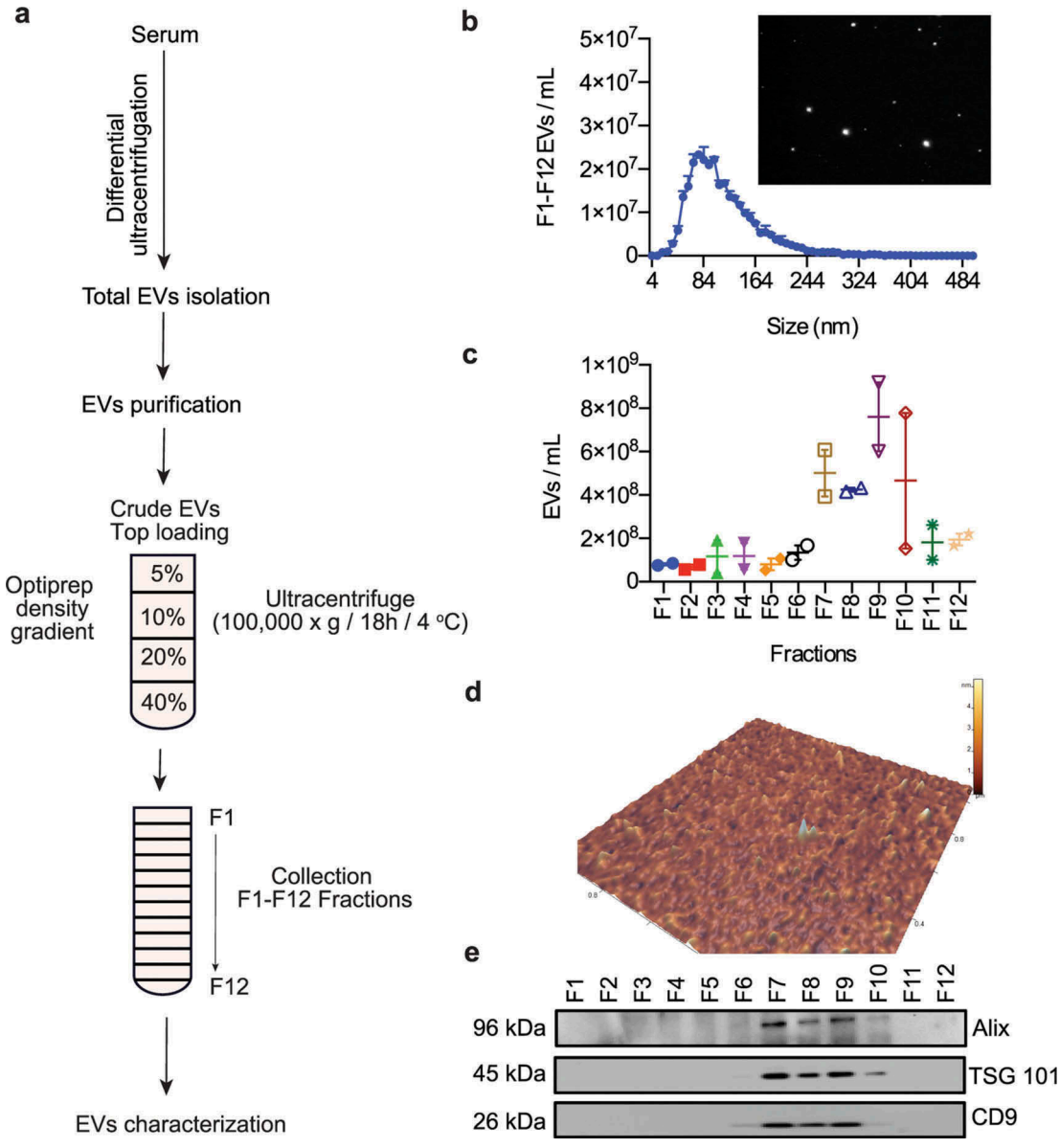

Figure 3. Isolation and characterization of EVs from rat serum. (a) Extracellular Vesicle (EVs) isolation and purification procedure by ultracentrifugation. EVs obtained after centrifugation at 100,000 x g were resuspended, top-loaded on a 5–40% on iodixanol (Optiprep) and ultracentrifuge at 100,000 x g for 18 h. Twelve 1 mL fractions (F1–F12) were collected. (b) Size distribution graph shows the distribution of F1-F12 EVs fractions in the size range of 4–500 nm from WT-rats (n = 2). Inset showing representative EVs morphology captured from the video in zeta view. (c) Final concentration of EVs obtained from 6 wild-type rats pooled serum (n = 2; n refers to pooled serum from 3 rats and represented by one symbol) for each fraction (F1-F12) followed by density gradient ultracentrifugation was analysed by Zeta View. (d) Atomic force microscopy (AFM) image of pooled F6-F10 fractions EVs. (e) Proteins from each fraction (F1-F12) of and F1-12 EVs were analysed by western blot for the presence of EV-associated proteins ALIX, TSG101 and CD9.

seropositive individuals [5]. The data presented in this study demonstrate a significant enrichment of neuronal origin EVs (L1CAM^{+} EVs) in the extracellular space of the brain with also a concomitant increase of these in the sera of HIV-1 Tg rats compared to the WT animals. In accordance with previous studies demonstrating that HIV-1 infected individuals display increased plasma EVs compared with healthy controls (Hubert et al., 2015), we also identified increased numbers of circulating total EVs in the HIV-1 Tg rat compared with the WT group.

The choice of animal models in studying HAND has been fraught with limitations since HIV-1 does not infect rodents. While none of the models developed can recapitulate the human syndrome of HAND, several small animal models have been exploited to address specific questions and aspects of HAND pathogenesis

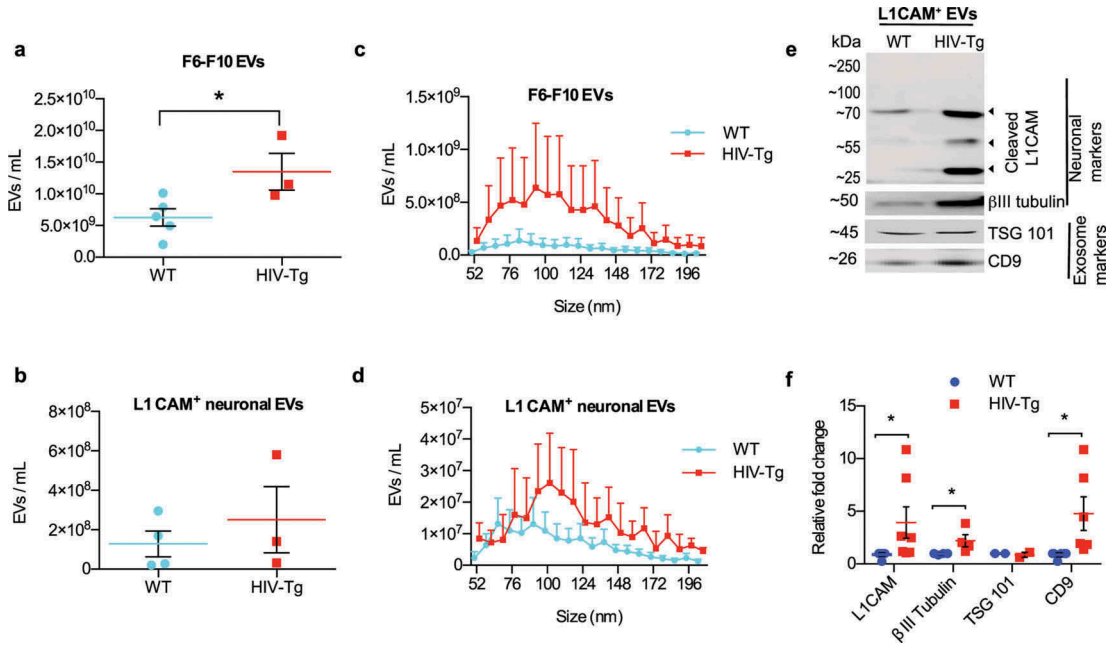

Figure 4. Neuronal EVs are enriched in the sera of transgenic rats. (a) Graph shows the concentration of EVs (F6-F10 fractions) isolated from equal amount of pooled sera from WT rats (n = 5, each n is equivalent to pooled serum of 3–4 rats) and HIV-1 Tg rats (n = 3, each n is equivalent to pooled serum of 3–4 rats). All conditions and dilutions were kept identical for both the groups (Wt and HIV-1 Tg) for further isolation of F6-F10 EVs and L1CAM$^+$ EVs. * $p < 0.05$ by unpaired parametric student's t-test with equal standard deviation. (b) Graph shows the concentration of EVs from the L1CAM$^+$ EVs fractions using zeta view and obtained from immunoprecipitation of pooled F6-F10 fractions of Wt and HIV-1 Tg rats (n = 3, each n is equivalent to pooled serum of 3–4 rats). (c) Size distribution of F6-F10 fractions and (d) L1CAM$^+$EVs was examined using zeta view. Figures depict the actual concentration of EVs by adjusting with the dilution factor in the range of 50–200 nm. (e) Western blot images show increased expression of neuronal markers (L1CAM, βIII Tubulin) in L1CAM$^+$ EVs from HIV-1 Tg rats when compared to L1CAM$^+$ EVs from WT rats. Equal amount of serum was used as the starting material to derive L1CAM$^+$ EVs. Equal volume of EVs (40 uL) after adjusting the obtained L1CAM$^+$ volume to equal to parent F6-F10 EVs fraction was used to load the gel. TSG 101 and CD9 were used as positive controls for exosome marker. (f) Densitometry of the proteins in relation to WT rats. Graph for L1CAM expression shows densitometry of ~55 kDa band. * $p < 0.05$ by unpaired parametric student's t-test using Mann-Whitney test.

[48,49]. Herein we chose to focus on the HIV-1 Tg rats that constitutively express 7 of the 9 viral proteins throughout the lifespan. These rats ideally mimic the human scenario of HIV-1-infection in the presence of cART, with substantially suppressed viraemia but ongoing presence of viral proteins even in the CNS, resulting likely from the ongoing low-level virus replication in viral reservoirs [50,51]. Another advantage of these rats is their ability to recapitulate some of the behavioural cognitive deficits of HAND [34,35,52]. Despite its utility in studying HAND, and allowing us to assess the impact of viral proteins on HAND, one of the major limitations of this model is that it is not an infectious model, thus necessitating the importance of validating our findings in more relevant model system. We thus sought to confirm our rodent findings in the serum of HIV+ patients on cART. Similar to findings in the rat model, a previous study by Chettimada et al. demonstrated elevated levels of EVs and exosomal markers in the plasma of HIV-1 infected patients compared to that of the healthy controls [53].

For this study, we chose to use a combination of EV isolation and purification methods involving both differential ultracentrifugation as well as the well-established iodixanol (Optiprep) gradient ultracentrifugation approaches from the brain and serum, and also followed the minimal information for studies of extracellular vesicles 2018 (MISEV2018) guidelines for EV characterization [38,40]. Previous studies have reported the use of other isolation/purification methods such as precipitation solution-based ExoQuick and total exosome isolation. A study performed by Van Deun et al., demonstrated elevated levels of exosomal marker proteins (Alix, HSP90α, HSP70, TSG101, and CD63) by western blot analysis in lysates from centrifugation-based (ultracentrifugation and optiprep density gradient) methods compared with the precipitation solution-based ExoQuick and total exosome isolation methods [54].

Neuronal enrichment of EVs (L1CAM$^+$ EVs) has been suggested to improve the signal to noise ratio and lower the detection threshold when assessing brain-specific serum EV expression in several

neurodegenerative diseases [29,43,55]. The 220-kDa full-length molecule L1CAM is proteolytically processed at different sites by different enzymes, leading to generation of differently sized cleaved products of ~140, ~80, ~70, ~55 and ~30 kDa, and serves as a substrate for regulating intramembrane proteolysis [46,56,57]. Ectodomain shedding of L1CAM yields a C-terminal stub (L1-32), which is retained in the plasma membrane [57], with the ectodomain cleavage of membrane molecules accelerated under pathological conditions involving neurodegeneration [58]. Lutz et al. showed that the 70 kDa fragment generated from serine protease-dependent cleavage of full-length L1CAM at the plasma membrane was transported from the plasma membrane to a late endosomal compartment cleavage with alterations in the levels of the fragment that were found to be associated with neurodegeneration [56]. The 70 kDa L1CAM fragment can also be cleaved into a sumoylated ~30 kDa cytosolic fragment [46]. To detect the biotinylated fragment after its release in EVs, biotinylated proteins were isolated from these fractions using streptavidin beads and analysed for the presence of the biotinylated fragments by western blot analysis using c-terminal antibody. Interestingly, we observed the L1CAM cleaved form (~ 70, ~55 and ~30 kDa) in L1CAM$^+$ EVs derived from both brain and sera, suggesting the ectodomain cleavage of full-length L1CAM, as previously reported [46,47]. Similar to our findings, L1CAM fragment of 55 kDa was also observed in EVs isolated from cell culture supernatants after cell surface biotinylation and L1 stimulation of neuroblastoma cells [56]. We also confirmed the L1CAM$^+$ EVs for their neuronal origin by assessing for another neuronal marker βIII tubulin. We observed an increase in purified EVs and L1CAM$^+$ neuronal EVs in both the brain and sera of HIV-1 Tg rats compared with the WT rats, thereby suggesting increased shedding and transport in the periphery of the neuronal origin EVs in the context of viral proteins.

In this study, we demonstrate the feasibility of L1CAM$^+$ EV isolation from the brain and sera of HIV-1 Tg rats, suggesting use of HIV-1 Tg rats as a viable model for future studies involving EV signalling in HIV-associated brain injury. Circulating neuronal exosomes hold a great promise to evaluate the neurotoxicity, pathophysiology of neurons and progressive neurodegeneration prior to the development of symptoms.

Acknowledgments

This work was supported by National Institutes of Health, National Institute on Drug Abuse grants DA035203, DA040397, DA041751, DA044586 (to S. Buch); DA043138 (to S. Buch and G. Hu); and DA046831 and DA042704 (to G. Hu); and National Institute of Mental Health grants MH106425 (to S. Buch) and MH112848 (to S. Buch and G. Hu), as well as the Nebraska Center for Substance Abuse Research. The project was supported by National Institutes of Health, National Institute of Mental Health grant 2P30MH062261. The content is solely the responsibility of the authors and does not necessarily represent the official views of the National Institutes of Health.

Disclosure statement

No potential conflict of interest was reported by the authors.

Funding

This work was supported by the National Institute of Mental Health [MH106425 and MH112848];National Institute on Drug Abuse [DA046831 and DA042704];National Institute on Drug Abuse [DA035203, DA040397, DA041751, DA044586, DA043138].

ORCID

Ke Liao http://orcid.org/0000-0002-3475-9598
Fang Niu http://orcid.org/0000-0002-5035-7409
Eric S. Peeples http://orcid.org/0000-0002-2892-2678
Shilpa Buch http://orcid.org/0000-0002-3103-6685

References

[1] Ko A, Kang G, Hattler JB, et al. Macrophages but not astrocytes harbor HIV DNA in the brains of HIV-1-Infected aviremic individuals on suppressive antiretroviral therapy. J Neuroimmune Pharmacol. 2019;14:110–119.
[2] Heaton RK, Clifford DB, Franklin DR Jr., et al. HIV-associated neurocognitive disorders persist in the era of potent antiretroviral therapy: CHARTER study. Neurology. 2010;75:2087–2096.
[3] Nath A. Human immunodeficiency virus (HIV) proteins in neuropathogenesis of HIV dementia. J Infect Dis. 2002;186(Suppl 2):S193–198.
[4] Mediouni S, Darque A, Baillat G, et al. Antiretroviral therapy does not block the secretion of the human immunodeficiency virus tat protein. Infect Disord Drug Targets. 2012;12:81–86.
[5] Heaton RK, Franklin DR, Ellis RJ, et al. HIV-associated neurocognitive disorders before and during the era of combination antiretroviral therapy: differences in rates, nature, and predictors. J Neurovirol. 2011;17:3–16.
[6] Chan P, Hellmuth J, Spudich S, et al. Cognitive impairment and persistent CNS injury in treated HIV. Curr HIV/AIDS Rep. 2016;13:209–217.
[7] Eggers C, Arendt G, Hahn K, et al. HIV-1-associated neurocognitive disorder: epidemiology, pathogenesis, diagnosis, and treatment. J Neurol. 2017;264:1715–1727.
[8] Clifford DB, Ances BM. HIV-associated neurocognitive disorder. Lancet Infect Dis. 2013;13:976–986.

[9] Hu G, Yang L, Cai Y, et al. Emerging roles of extracellular vesicles in neurodegenerative disorders: focus on HIV-associated neurological complications. Cell Death Dis. 2016;7:e2481.
[10] Quek C, Hill AF. The role of extracellular vesicles in neurodegenerative diseases. Biochem Biophys Res Commun. 2017;483:1178–1186.
[11] Buschmann D, Kirchner B, Hermann S, et al. Evaluation of serum extracellular vesicle isolation methods for profiling miRNAs by next-generation sequencing. J Extracell Vesicles. 2018;7:1481321.
[12] Izadpanah M, Seddigh A, Ebrahimi Barough S, et al. Potential of extracellular vesicles in neurodegenerative diseases: diagnostic and therapeutic indications. J Mol Neurosci. 2018;66:172–179.
[13] Fruhbeis C, Frohlich D, Kramer-Albers EM. Emerging roles of exosomes in neuron-glia communication. Front Physiol. 2012;3:119.
[14] Hu G, Liao K, Niu F, et al. Astrocyte EV-Induced lincRNA-Cox2 regulates microglial phagocytosis: implications for morphine-mediated neurodegeneration. Mol Ther Nucleic Acids. 2018;13:450–463.
[15] Chaudhuri AD, Dastgheyb RM, Yoo SW, et al. TNFalpha and IL-1beta modify the miRNA cargo of astrocyte shed extracellular vesicles to regulate neurotrophic signaling in neurons. Cell Death Dis. 2018;9:363.
[16] Schwab A, Meyering SS, Lepene B, et al. Extracellular vesicles from infected cells: potential for direct pathogenesis. Front Microbiol. 2015;6:1132.
[17] Hu G, Gong AY, Roth AL, et al. Release of luminal exosomes contributes to TLR4-mediated epithelial antimicrobial defense. PLoS Pathog. 2013;9:e1003261.
[18] Hu G, Drescher KM, Chen XM. Exosomal miRNAs: biological properties and therapeutic potential. Front Genet. 2012;3:56.
[19] Shi M, Sheng L, Stewart T, et al. New windows into the brain: central nervous system-derived extracellular vesicles in blood. Prog Neurobiol. 2019;175:96–106.
[20] Schiera G, Di Liegro CM, Di Liegro I. Extracellular membrane vesicles as vehicles for brain cell-to-cell interactions in physiological as well as pathological conditions. Biomed Res Int. 2015;2015:152926.
[21] Alvarez-Erviti L, Seow Y, Yin H, et al. Delivery of siRNA to the mouse brain by systemic injection of targeted exosomes. Nat Biotechnol. 2011;29:341–345.
[22] Liao K, Niu F, Dagur RS, et al. Intranasal delivery of lincRNA-Cox2 siRNA loaded extracellular vesicles decreases lipopolysaccharide-induced microglial proliferation in mice. J Neuroimmune Pharmacol. 2019. https://doi.org/10.1007/s11481-019-09864-z
[23] Zhuang X, Xiang X, Grizzle W, et al. Treatment of brain inflammatory diseases by delivering exosome encapsulated anti-inflammatory drugs from the nasal region to the brain. Mol Ther. 2011;19:1769–1779.
[24] Gamez-Valero A, Beyer K, Borras FE. Extracellular vesicles, new actors in the search for biomarkers of dementias. Neurobiol Aging. 2019;74:15–20.
[25] Pulliam L, Sun B, Mustapic M, et al. Plasma neuronal exosomes serve as biomarkers of cognitive impairment in HIV infection and Alzheimer's disease. J Neurovirol. 2019;25:702–709.
[26] Rathjen FG, Schachner M. Immunocytological and biochemical characterization of a new neuronal cell surface component (L1 antigen) which is involved in cell adhesion. Embo J. 1984;3:1–10.
[27] Lown JA, Barr AL, Kelly A. Auto anti-M antibody following renal transplantation. Vox Sang. 1980;38:301–304.
[28] Faure J, Lachenal G, Court M, et al. Exosomes are released by cultured cortical neurones. Mol Cell Neurosci. 2006;31:642–648.
[29] Mustapic M, Eitan E, Werner JK Jr., et al. Plasma extracellular vesicles enriched for neuronal origin: a potential window into brain pathologic processes. Front Neurosci. 2017;11:278.
[30] Lazar I, Clement E, Ducoux-Petit M, et al. Proteome characterization of melanoma exosomes reveals a specific signature for metastatic cell lines. Pigment Cell Melanoma Res. 2015;28:464–475.
[31] Liang B, Peng P, Chen S, et al. Characterization and proteomic analysis of ovarian cancer-derived exosomes. J Proteomics. 2013;80:171–182.
[32] Lamontagne-Proulx J, St-Amour I, Labib R, et al. Portrait of blood-derived extracellular vesicles in patients with Parkinson's disease. Neurobiol Dis. 2019;124:163–175.
[33] Reid W, Sadowska M, Denaro F, et al. An HIV-1 transgenic rat that develops HIV-related pathology and immunologic dysfunction. Proc Natl Acad Sci U S A. 2001;98:9271–9276.
[34] Peng J, Vigorito M, Liu X, et al. The HIV-1 transgenic rat as a model for HIV-1 infected individuals on HAART. J Neuroimmunol. 2010;218:94–101.
[35] Vigorito M, Connaghan KP, Chang SL. The HIV-1 transgenic rat model of neuroHIV. Brain Behav Immun. 2015;48:336–349.
[36] Sundermann EE, Heaton RK, Pasipanodya E, et al. Sex differences in HIV-associated cognitive impairment. AIDS. 2018;32:2719–2726.
[37] Sampey GC, Meyering SS, Zadeh MA, et al. Exosomes and their role in CNS viral infections. J Neurovirol. 2014;20:199–208.
[38] Hurwitz SN, Sun L, Cole KY, et al. An optimized method for enrichment of whole brain-derived extracellular vesicles reveals insight into neurodegenerative processes in a mouse model of Alzheimer's disease. J Neurosci Methods. 2018;307:210–220.
[39] Coumans FAW, Brisson AR, Buzas EI, et al. Methodological guidelines to study extracellular vesicles. Circ Res. 2017;120:1632–1648.
[40] Thery C, Witwer KW, Aikawa E, et al. Minimal information for studies of extracellular vesicles 2018 (MISEV2018): a position statement of the international society for extracellular vesicles and update of the MISEV2014 guidelines. J Extracell Vesicles. 2018;7:1535750.
[41] Narayanan A, Iordanskiy S, Das R, et al. Exosomes derived from HIV-1-infected cells contain trans-activation response element RNA. J Biol Chem. 2013;288:20014–20033.
[42] Iwai K, Minamisawa T, Suga K, et al. Isolation of human salivary extracellular vesicles by iodixanol density gradient ultracentrifugation and their characterizations. J Extracell Vesicles. 2016;5:30829.

[43] Fiandaca MS, Kapogiannis D, Mapstone M, et al. Identification of preclinical Alzheimer's disease by a profile of pathogenic proteins in neurally derived blood exosomes: a case-control study. Alzheimers Dement. 2015;11:600–607 e601.
[44] Sun B, Dalvi P, Abadjian L, et al. Blood neuron-derived exosomes as biomarkers of cognitive impairment in HIV. AIDS. 2017;31:F9–F17.
[45] DeMarino C, Pleet ML, Cowen M, et al. Antiretroviral drugs alter the content of extracellular vesicles from HIV-1-infected cells. Sci Rep. 2018;8:7653.
[46] Kakad PP, Penserga T, Davis BP, et al. An ankyrin-binding motif regulates nuclear levels of L1-type neuroglian and expression of the oncogene Myc in Drosophila neurons. J Biol Chem. 2018;293:17442–17453.
[47] Mechtersheimer S, Gutwein P, Agmon-Levin N, et al. Ectodomain shedding of L1 adhesion molecule promotes cell migration by autocrine binding to integrins. J Cell Biol. 2001;155:661–673.
[48] Gorantla S, Poluektova L, Gendelman HE. Rodent models for HIV-associated neurocognitive disorders. Trends Neurosci. 2012;35:197–208.
[49] Joseph J. Optimizing animal models for HIV-associated CNS dysfunction and CNS reservoir research. J Neurovirol. 2018;24:137–140.
[50] Letendre S. Central nervous system complications in HIV disease: HIV-associated neurocognitive disorder. Top Antivir Med. 2011;19:137–142.
[51] Dahl V, Peterson J, Fuchs D, et al. Low levels of HIV-1 RNA detected in the cerebrospinal fluid after up to 10 years of suppressive therapy are associated with local immune activation. AIDS. 2014;28:2251–2258.
[52] Rowson SA, Harrell CS, Bekhbat M, et al. Neuroinflammation and behavior in HIV-1 transgenic rats exposed to chronic adolescent stress. Front Psychiatry. 2016;7:102.
[53] Chettimada S, Lorenz DR, Misra V, et al. Exosome markers associated with immune activation and oxidative stress in HIV patients on antiretroviral therapy. Sci Rep. 2018;8:7227.
[54] Van Deun J, Mestdagh P, Sormunen R, et al. The impact of disparate isolation methods for extracellular vesicles on downstream RNA profiling. J Extracell Vesicles. 2014;3:24858–24871.
[55] Guix FX, Corbett GT, Cha DJ, et al. Detection of aggregation-competent tau in neuron-derived extracellular vesicles. Int J Mol Sci. 2018;19:663–685.
[56] Lutz D, Wolters-Eisfeld G, Joshi G, et al. Generation and nuclear translocation of sumoylated transmembrane fragment of cell adhesion molecule L1. J Biol Chem. 2012;287:17161–17175.
[57] Kiefel H, Bondong S, Hazin J, et al. L1CAM: a major driver for tumor cell invasion and motility. Cell Adh Migr. 2012;6:374–384.
[58] Hooper NM, Karran EH, Turner AJ. Membrane protein secretases. Biochem J. 1997;321(Pt 2):265–279.